

Impact of the Juan Fernandez ridge on the Pampean flat subduction inferred from full waveform inversion

Yajian Gao^{1,2}, Xiaohui Yuan¹, Benjamin Heit¹, Frederik Tilmann^{1,2},
Dirk-Philip van Herwaarden³, Solvi Thrastarson³, Andreas Fichtner³, Bernd
Schurr¹

¹GFZ German Research Centre for Geosciences, Potsdam, Germany

²Freie Universität Berlin, Berlin, Germany

³ETH Zürich, Zürich, Switzerland

Key Points:

- A new seismic model for the crust and upper mantle beneath central Chile and western Argentina is presented.
- Thinning and tearing within the Pampean flat slab is detected along the inland projection of the Juan Fernandez Ridge.
- A relic slab is imaged beneath the Pampean flat slab, reflecting slab break-off during the flattening process.

Corresponding author: Yajian Gao, yjgao@gfz-potsdam.de

Abstract

A new seismic velocity model for the south Central Andes is derived from full waveform inversion, covering the Pampean flat and adjacent Payenia steep subduction segments. Strong focused crustal low-velocity anomalies indicate partial melts in the Payenia segment along the volcanic arc, whereas weaker low-velocity anomalies covering a wide zone in Pampean possibly indicates remnant melts in the past. Thinning and tearing of the flat Nazca slab below the Pampean is inferred by gaps in the high-velocity slab along the inland projection of the Juan-Fernandez-Ridge. A high-velocity anomaly in the upper mantle below the flat slab is interpreted as a relic Nazca slab segment, which indicates an earlier slab break-off during the flattening process, triggered by the buoyancy of the Juan-Fernandez-Ridge. In Payenia, large-scale low-velocity anomalies atop and below the re-steepened Nazca slab are associated with the re-opening of the mantle wedge and sub-slab asthenospheric flow, respectively.

Plain Language Summary

Taking advantage of the abundant information recorded in seismic waveforms, we imaged the seismic structure of the crust and upper mantle beneath central Chile and western Argentina, where the oceanic Nazca slab is subducting beneath the South American plate. The Nazca plate is almost flat in the north of the study area below the Pampean region, where the Juan Fernandez seamount ridge is attached on the subducting Nazca slab. The slab steepens again in the south in the Payenia region. Our model reveals pronounced low-velocity anomalies in the middle of the Pampean flat slab along the inland projection of the Juan Fernandez Ridge, indicating that the Pampean flat slab is thinned or even torn apart. A high-velocity anomaly is imaged beneath the flat slab, representing a former slab segment that was broken off during the slab flattening process and was overridden by the advancing young slab. Our model suggests a causal relationship between the oceanic ridge subduction and the flat slab formation. In the Payenia region, the slab re-steepening resulted in the re-establishment of the mantle wedge and induced subslab asthenospheric flow, which are characterized by low-velocity anomalies in the model.

1 Introduction

The causes and consequences of flat subduction along the South American western margin are vigorously debated (e.g., Gutscher et al., 2000; Ramos & Folguera, 2009). Two promi-

47 nent on-going flat subduction segments beneath the Andes are the Peruvian and Pampean
 48 flat subduction zones, north and south of the conspicuous kink in the South American
 49 coastline respectively. They have been documented based on seismology (e.g., Wagner et
 50 al., 2005; Pesicek et al., 2012), volcanism (e.g. S. M. Kay & Abbruzzi, 1996; S. M. Kay
 51 & Mpodozis, 2002), gravity modeling (e.g. Sánchez et al., 2019) and electrical conductiv-
 52 ity measurements (e.g. Burd et al., 2013, 2014). Scenarios for their formation have been
 53 explored with geodynamic modeling (e.g., Hu et al., 2016; Hu & Liu, 2016). In this study
 54 we focus on the Pampean flat subduction and Payenia steep subduction to the south, from
 55 28°–38°S. Here, the Nazca slab is subducting beneath central Chile and western Argentina
 56 with a convergence rate of $\sim 6.7 \text{ cm a}^{-1}$ in the N78°E direction (Kendrick et al., 2003). In
 57 the Pampean flat subduction zone, the Nazca slab propagates horizontally for 200-300 km
 58 beneath the southern Central Andes (Figure 1a). There is no consensus on a single mech-
 59 anism for triggering flat subductions, but the following mechanisms have been proposed:
 60 (1) Increased buoyancy related to the presence of seamount chains or oceanic plateaus or
 61 younger age of the slab (e.g., Gans et al., 2011; Huangfu et al., 2016; Hu et al., 2016; S. Liu
 62 & Currie, 2016); (2) plate suction forces from a cold and/or over-thickened overriding plate
 63 with increased viscosity (e.g., Manea et al., 2012; Rodríguez-González et al., 2012); (3) in-
 64 creased movement of the overriding plate towards the trench and trench retreat (Schepers
 65 et al., 2017; Manea et al., 2017; S. Liu & Currie, 2016); (4) Over-pressure below the slab
 66 induced by mantle plumes (Boutelier & Cruden, 2008; Rodríguez-González et al., 2014).
 67 The Pampean flat subduction zone is believed to be associated with the subduction of the
 68 Juan Fernandez seamount ridge (JFR, Figure 1) (e.g. Gutscher et al., 2000; S. M. Kay
 69 & Mpodozis, 2002; Ramos et al., 2002). Plate reconstructions (Yáñez et al., 2001; Bello-
 70 González et al., 2018) indicate that the ridge has been moving southward along the western
 71 margin of South America. It was subducting beneath the Altiplano and Puna plateaus
 72 (21°–26°S) at $\sim 40\text{--}20 \text{ Ma}$, inducing inland migration of volcanism and a temporary lull be-
 73 tween 20–12 Ma (Yáñez et al., 2001; S. M. Kay & Coira, 2009; Beck et al., 2015). The
 74 JFR arrived at the current position beneath the Sierras Pampeanas around 12 Ma (Figure
 75 1) and the related flat subduction of the Nazca slab has triggered inland migration and
 76 spatial expansion of subduction-related volcanism (S. M. Kay & Mpodozis, 2002), uplift of
 77 the main Andes, thick-skinned deformation, crustal thickening and basement uplift over a
 78 broad zone in the overriding plate (Cristallini & Ramos, 2000; Ramos et al., 2002). The
 79 occurrence of adakitic magmatism has also been attributed to slab melting (Gutscher et al.,
 80 2000; Hu et al., 2016) or intrusion of the basaltic arc magmas (R. W. Kay & Kay, 2002).

In this study, we employ seismic full waveform inversion (FWI) to investigate the seismic structure in the upper mantle to understand the slab configuration changes and crustal melt distributions in response to the subduction of the JFR. For readability, we divide the whole study region into two domains (Figure 1a): the Pampean flat subduction zone in the north and the Payenia steep subduction zone in the south. The latter used to be a flat subduction zone from 15 Ma to 5 Ma but the slab has re-steepened since 4-5 Ma (S. M. Kay & Mpodozis, 2002; Ramos & Folguera, 2009).

2 Data and Method

Following the same workflow as Gao et al. (2021), we collected 139 earthquakes from the Global Centroid-Moment-Tensor (GCMT) catalog (Ekström et al., 2012), which were recorded by 19 seismic networks (Figure 1 and Figure S1) operating between 1996 to 2019 and magnitudes between M_W 5.0 to 7.0. Detailed network information and ray-path coverage are presented in the supplementary material (Figures S1–S2 and Table S1). Our seismic velocity model is the result of the multi-scale FWI based on the adjoint methodology (e.g., Fichtner et al., 2010; Tape et al., 2010), starting from the 3D seismic velocity model *S20RTS* (Ritsema et al., 2004). Solutions of the visco-elastic wave equation in a radially anisotropic Earth model are obtained from *Salvus* (Afanasyev et al., 2019). More information about the inversion workflow is provided in the supplementary material (Text S1).

In order to analyse the resolution of the inversion and trade-offs between the parameters, we calculated the Hessian-vector product $H\delta m$ as point-spread function to assess possible smearing and distortion (Fichtner & Trampert, 2011; Tao et al., 2018). We find that the isotropic V_S and V_P models are robustly determined in the resolved region with a spatial resolution of 30-40 km in the upper mantle and 20-25 km in the crust horizontally and vertically. Detailed resolution tests are described in Text S2 and Figure S18-S24.

3 Results and discussion

After 53 iterations of FWI, the crust and upper mantle structure beneath central Chile and western Argentina has been clearly imaged. We display the isotropic V_S model with some key depth and cross-sections. Further images and the isotropic V_P model are shown in the supplementary material (Figures S5–S16).

3.1 Multi-stage crustal partial melting and mantle wedge evolution

In contrast to the vigorous partial melting represented by strong low-velocity middle-crust beneath the Altiplano-Puna Volcanic Complex and volcanic arc for the northern Chile steep subduction zone (Yuan et al., 2000; Ward et al., 2014; Gao et al., 2021), the middle crust in the Pampean flat subduction zone (28°–33° S) exhibits only moderately low to normal velocities along the volcanic arc (Figure 2a).

Low-velocity anomaly C1 (Figure 2a and S17) is located beneath the Frontal Cordillera (FC) and has been reported by several earlier studies (e.g., Ward et al., 2013, 2017; Gao et al., 2021). C1 marks the waning partial melting beneath the Incapillo Caldera and Dome Complex (ICDC, Figure 1a), which is the southernmost ignimbritic caldera of the Central Andes during the Pleistocene (Goss et al., 2009, 2011). Meanwhile, weak and isolated low-velocity anomalies (C2 and C3, Figure 2a) beneath the Sierras Pampeanas (SP) are accompanied by middle to late Miocene adakitic volcanoes including the Famatina Mogotes Group (FMG, S. M. Kay & Mpodozis, 2002) and Gualcamayo Igneous Complex (GIC, D’Annunzio, Rubinstein, & Rabbia, 2018), indicating a slab melting origin or basaltic arc magma source (S. M. Kay & Abbruzzi, 1996; R. W. Kay & Kay, 2002; Gutscher et al., 2000; Hu & Liu, 2016).

A striking low-velocity anomaly C5 (Figure 2b and Profile (a) in Figure 3) at approximate Moho depth (60 km) extends from the Frontal Cordillera to the Sierras Pampeanas (SP), forming a thin layer above the Pampean flat slab. As the mantle wedge must have been thinned to a sliver or completely closed during the flattening of the Nazca slab (Gutscher et al., 2000; Manea et al., 2017), this low-velocity anomaly could be attributed to the combined effect of a fossil ‘MASH’ zone (melting-assimilation-storage-homogenization) and modern fluids released from the current flat slab (Hildreth & Moorbath, 1988). Dehydration of the flat slab has the potential to significantly modify the overriding lithosphere above it for a long distance from the trench (Z. Li, 2020). In Figure 3a-c, the continental mantle lithosphere south of 28°S appears to be thinned considerably or even displaced (Axen et al., 2018; Gutscher, 2018).

In contrast, south of 33°S, C4 may mark the restoration of partial melt accumulation in the middle crust during the re-steepening process of the Nazca slab beneath the Payenia (Marot et al., 2014; Ramos & Folguera, 2009). The late Miocene volcanic activity in the back-arc and Pleistocene-Holocene volcanic activity in the frontal arc (including large-scale Payenia Volcanic Province, Figure 1a) indicate a trench-ward migration of the volcanism.

Following the re-steepening of the slab since 4-5 Ma, the mantle wedge has re-opened, leading to the re-injection of hot asthenosphere and renewed melt formation in the wedge induced by slab-derived fluids dehydration, in turn inducing trench-ward migration of the volcanism (Gutscher et al., 2000; S. M. Kay & Mpodozis, 2002; Ramos & Folguera, 2009, 2011; Marot et al., 2014). The re-opened mantle wedge is clearly imaged in our model as low-velocity anomaly M3 and represents the present situation after the slab re-steepening (Figure 2c and profile (d) and (e) in Figure 3).

3.2 Slab thinning and tearing along the Juan Fernandez Ridge

In the central part of the Pampean flat slab, two low-velocity anomalies (M1 and M2) span a slab window along the inland projection of the JFR (Figure 2c and Profile (b) in Figure 3) and are surrounded by two high-velocity limbs of the flat slab (H2). Though many prior works detected the Pampean flat slab with strong heterogeneities, most of seismological studies focused on the seismic structure south of 29°S (e.g., Wagner et al., 2005; Porter et al., 2012; Marot et al., 2014; Linkimer et al., 2020), leaving an observational gap from 27°–29°S. In this study, events and stations north of 27°S are included in the inversion, allowing us to resolve M1 and M2.

The inland projection of the JFR is not well constrained from previous plate reconstruction studies (Yáñez et al., 2001; Bello-González et al., 2018) due to its relatively long subduction and migration history (12 Ma) beneath the Pampean area. Hence, the extent of the region affected by the JFR is not known precisely, nor are details of the seismic structure associated with the JFR (Gutscher et al., 2000; Wagner et al., 2005; Gans et al., 2011; Marot et al., 2014; Haddon & Porter, 2018). Following S. M. Kay and Mpodozis (2002), we assume the uncertainty width of the influence zone of the JFR within the oceanic lithosphere is 200 km, which also takes into account the region of underplating and possible hydration of the oceanic lithosphere (Kopp et al., 2004), which extends beyond the seamount chain itself. Thus, the low-velocity anomalies M1 and M2 are located within the JFR influence range. Similar to predictions from numerical modelling (Hu & Liu, 2016), the slab thinning and tearing zone develops within the central part of the current flat slab. In Hu & Liu’s model, slab thinning and tearing initiates from the inboard tip of the flat slab before re-steepening downdip and propagates trench-wards, parallel to the track of the JFR and consistent our direct observation. In addition to the enhanced buoyancy of the JFR, its hydration state and inherited normal faults (Kopp et al., 2004) might have caused zones of weakness along which the thinning and tearing could progress.

Conspicuously, the slab tearing zone (M1 and M2) is characterized by the absence of intra-slab seismicity, in contrast to the slab limbs to the north and south (Fig. 2c). The focal mechanisms show a clear asymmetric pattern across the JFR track: the north branch of H2 is characterized by predominantly NE-SW oriented T axes, which are subparallel to the track of the JFR, whereas the T axes for events in the southern branch of H2 are oriented mainly NW-SE, sub-normal to the JFR trend, implying a $\sim 90^\circ$ rotation of T axes across the aseismic zone (Figure 2c) at 120-160 km at depth. The northeast extension in the northern slab limb parallel to the JFR is superimposed on dominant slab pull (downdip extension), which is also reflected in the velocity field (Hu & Liu, 2016) and azimuthal anisotropy (Hu et al., 2017; Lynner et al., 2017). The south branch is coincident with the track of the JFR and attributed to the reactivation of the preexisting normal faults, causing vigorous intra-slab seismicity (Ranero et al., 2005; Anderson et al., 2007; Gans et al., 2011; Ammirati et al., 2015; Wagner et al., 2020).

Near the slab tearing zone, Heit et al. (2008) detected a strong oceanic LAB signal west of 69°W that suddenly disappears and even changes polarity further east (Profile (c) in Figure 3). Recent magnetic and gravity modeling work (Sánchez et al., 2019) also inferred hot asthenospheric flow beneath the flat slab and local slab thinning. These observations further validate our interpretation of M1 and M2 as evidence for thinning and tearing of the slab (Figure 4). M1 and M2 are also accompanied by weak crustal low-velocity anomalies C3 and C2 below the late Miocene adakitic volcanism including the GIC (D'Annunzio et al., 2018) and FMG (S. M. Kay & Mpodozis, 2002), respectively (Figure 2a), confirming enhanced slab melting (S. M. Kay & Mpodozis, 2002; Gutscher et al., 2000; Hu & Liu, 2016) near the tearing zone (Figure 4a).

The Pampean flat slab, after having developed in the Middle to Late Miocene, suffered from numerous instabilities, such as internal stresses induced by the increased buoyancy of the JFR relative to its two flanks, changes in hydration state, reactivation of inherited normal faults, and basal heating by asthenosphere flow (Rodríguez-González et al., 2014). These factors have induced weakening, thinning and finally tearing of the oceanic slab, followed by melting of the oceanic crust as predicted by the geodynamic model (Hu & Liu, 2016). The basalt input from the melted oceanic crust leads to the adakitic volcanism (Gutscher et al., 2000) during the late Miocene (Figure 4a).

3.3 Slab break-off: transition from steep to flat subduction?

A prominent high-velocity anomaly (H3) is found just below the flat Nazca slab (H2), extending from 28° S to 30° S (Figure 2d). At depth, H3 is dipping steeply to the east from 200 km down to 350 km depth (Profile (a), Figure 3). This anomaly was also visible in previous global or teleseismic tomography studies, but was so far not interpreted (e.g. C. Li et al., 2008; Portner et al., 2020; Mohammadzaheri et al., 2021). Recent S-wave teleseismic work (Rodríguez et al., 2021) captured a similar but larger-scale high-velocity anomaly extending from 200 km down to the lower mantle and attributed it to a part of relic Phoenix/Aluk plate, which was completely subducted by the late Cretaceous (Horton, 2018; Gianni et al., 2018). However, the resolution of the aforementioned models is limited in the upper mantle due to vertical smearing. We prefer to relate this anomaly to the more recent Nazca plate subduction as it seems unlikely that a part of the Phoenix slab could remain in the upper mantle for more than 100 million years and has not sunk into the lower mantle or thermally equilibrated with the surrounding mantle (Ramos & Folguera, 2009; Bello-González et al., 2018; Chen et al., 2019). Thus, we propose this anomaly to be a fossil fragment of the Nazca slab that was subducting steeply prior to the onset of flattening, indicating break-off from the leading edge of the current Nazca slab (S. Liu & Currie, 2016). Slab break-off during the slab flattening process is common in geodynamic models (e.g. Haschke et al., 2002; S. Liu & Currie, 2016; X. Liu & Currie, 2019; Dai et al., 2020). The conditions for slab break-off during the slab flattening process include fast trenchward migration of the overriding plate (high convergence rate) and a strong buoyancy contrast between either an oceanic plateau or aseismic ridge crust (here the JFR) and the normal thickness oceanic crust of an old slab (Haschke et al., 2002; Z. Li et al., 2011; S. Liu & Currie, 2016; X. Liu & Currie, 2019). The removal of the leading dense portion would allow the positive buoyancy of the trailing edge to quickly flatten out the slab (Figure 4b). In many global tomography models, the Nazca slab extends to much shallower depth in the south than the north, where it is visible down to 1000 km depth (C. Li et al., 2008; Obayashi et al., 2013). Several teleseismic tomography models (Portner et al., 2017, 2020; Rodríguez et al., 2021) for South America seem to indicate a slab hole at 200-300 km depth around 32°S in the re-steepened portion within the upper mantle. Thus the relic slab break-off or detachment from the head of the young and buoyant Nazca slab seems a viable option.

Taking account of the initial time of the transition from the steep to the flat subduction around 12 Ma coeval with the subduction of the JFR (Yáñez et al., 2001; S. M. Kay & Mpodozis, 2002; Ramos & Folguera, 2009), this would also be the time for the high density

portion ahead of the JFR to break off from the leading edge of the young Nazca slab (Figure 4b). Furthermore, partial eclogitization of the oceanic crust before the onset of the flat subduction may play an important role in controlling the breaking-off time (X. Liu & Currie, 2019) and sinking depth in the upper mantle. Thus, the tail of the broken portion would sink slowly in the upper mantle due to its relatively young age, while the head would have already sunk into the mantle transition zone or deeper, below the resolution limit of our model. After break-off, the young and buoyant Nazca slab with the JFR could lift to extend horizontally eastwards for nearly 300 km before re-steepening with a steep angle to a relatively shallower depth compared to the dip subduction zone north of 28° S (Figure 4b).

3.4 Subslab asthenospheric flow induced by sudden re-steepening of the Nazca slab beneath the Payenia?

Another striking feature in our model is the low-velocity anomaly M4 extending from 32°–36°S below the steep Nazca slab in Payenia subduction zone and from slab depths to 250–300 km depth (Figures 2c and 3, Profile. (e)-(h)). This low-velocity anomaly has also been observed by some earlier tomography studies (Feng et al., 2007; Portner et al., 2017, 2020; Celli et al., 2020; Rodríguez et al., 2021). Portner et al. (2017) attributed it to the asthenosphere entrainment by the JFR with the subducting Nazca slab due to the coupling between the asthenosphere and overlying oceanic lithosphere (L. Liu & Zhou, 2015). However, due to its large size and location, it may more likely be caused by hot asthenospheric flow induced by the sudden re-steepening of the Nazca slab and trench retreat (Ramos & Folguera, 2009; Lin, 2014; Hu et al., 2017; Mohammadzaheri et al., 2021) since 4 Ma beneath the Payenia subduction zone (Figure 4a).

4 Conclusions

Through multi-scale full seismic waveform inversion, we identify low velocity zones within the Pampean flat slab parallel to the inland projection of the Juan Fernandez Ridge, which we interpret as a tearing zone within the flat slab. It may be induced by the buoyancy contrast between the Pampean flat slab with Juan Fernandez Ridge attached and its surrounding steep slab portions to the north and south. Meanwhile, the buoyancy contrast between the young Nazca slab and the preceding steep Nazca slab appears to have triggered the slab break-off from the leading edge of current Nazca slab. The resulting buoyancy increase could possibly sustain the long-distance flat subduction. Flat subduction also expelled the

mantle wedge and shut off partial melting, resulting in much reduced volcanic activity and presence of partial melt in the crust. Re-steepening of the Nazca slab beneath the Payenia subduction zone seems to have significantly perturbed the sub-slab asthenospheric flow and introduced large-scale mantle flow, as visible in large low-velocity zone both above and below the slab. Re-opening of the mantle wedge and injection of the asthenosphere induced by the re-steepening of the Nazca slab may have caused the re-accumulation of partial melts within the middle crust and volcanic arc trench-ward migration and reactivation.

Acknowledgments

We gratefully acknowledge fruitful discussions with Lara S. Wagner, Jiashun Hu, Lijun Liu, Xiaowen Liu, Guohui Li, Wei Li, Tuo Zhang, Youqiang Yu. This work was supported by the Swiss National Supercomputing Center (CSCS) in the form of computing time grants s868 and s1040. Yajian Gao is sponsored by Freie Universität Berlin - China Scholarship Council Programm. Dirk-Philip van Herwaarden and Solvi Thrastarson were supported by the European Research Council (ERC) under the EU's Horizon 2020 programme (grant No. 714069).

Data Availability

Waveform data and station meta data were downloaded using the ObsPy (Krischer et al., 2015) module through the International Federation of Digital Seismograph Networks (FDSN) webservices from GEOFON Data Management Center (<https://geofon.gfz-potsdam.de/waveform/archive/>) and Incorporated Research Institutions for Seismology Data Management Center (IRIS-DMC, <http://www.iris.edu/ds/nodes/dmc/>). Raw data of the temporary and permanent networks used in this study with FDSN codes including C (<https://www.fdsn.org/networks/detail/C/>); C1 (<https://doi.org/10.7914/SN/C1>); CX (<https://doi.org/10.14470/PK615318>); GT (<https://doi.org/10.7914/SN/GT>); IU (<https://doi.org/10.7914/SN/IU>); WA (<https://www.fdsn.org/networks/detail/WA/>); 2B (<https://doi.org/10.14470/70092361>); 3A (https://www.fdsn.org/networks/detail/3A_2010/); 3H (<https://doi.org/10.14470/8U7569253520>); G (<https://doi.org/10.18715/GEOSCOPE.G>); X6 (https://doi.org/10.7914/SN/X6_2007); XH (https://doi.org/10.7914/SN/XH_2008); XS (<https://doi.org/10.15778/RESIF.XS2010>); XY (https://doi.org/10.7914/SN/XY_2010); YC (https://doi.org/10.7914/SN/YC_2000); YM (https://doi.org/10.7914/SN/YM_2010); ZA (<https://doi.org/10.14470/MN7557778612>); ZB (<https://doi.org/10.14470/M06442843258>); ZE (<https://www.fdsn.org/networks/detail/ZE.2010/>);

ZL(<https://doi.org/10.7914/SN/ZL.2007>); ZP(https://www.fdsn.org/networks/detail/ZP_1999/); ZQ(https://www.fdsn.org/networks/detail/ZQ_2004/); ZW(<https://doi.org/10.14470/MJ7559637482>);

References

- Afanasiev, M., Boehm, C., Van Driel, M., Krischer, L., Rietmann, M., May, D. A., ... Fichtner, A. (2019). Modular and flexible spectral-element waveform modelling in two and three dimensions. *Geophysical Journal International*, 216(3), 1675–1692. doi: <https://doi.org/10.1093/gji/ggy469>
- Amante, C., & Eakins, B. W. (2009). *ETOPO1 Global Relief Model converted to PanMap layer format*. PANGAEA. doi: <https://doi.org/10.1594/PANGAEA.769615>
- Ammirati, J. B., Alvarado, P., & Beck, S. L. (2015). A lithospheric velocity model for the flat slab region of Argentina from joint inversion of Rayleigh wave phase velocity dispersion and teleseismic receiver functions. *Geophysical Journal International*, 202(1), 224–241. doi: <https://doi.org/10.1093/gji/ggv140>
- Anderson, M., Alvarado, P., Zandt, G., & Beck, S. L. (2007). Geometry and brittle deformation of the subducting Nazca Plate, Central Chile and Argentina. *Geophysical Journal International*, 171(1), 419–434. doi: <https://doi.org/10.1111/j.1365-246X.2007.03483.x>
- Axen, G. J., van Wijk, J. W., & Currie, C. A. (2018). Basal continental mantle lithosphere displaced by flat-slab subduction. *Nature Geoscience*, 11(12), 961–964. doi: <https://doi.org/10.1038/s41561-018-0263-9>
- Beck, S. L., Zandt, G., Ward, K. M., & Scire, A. (2015). Multiple styles and scales of lithospheric foundering beneath the Puna Plateau, central Andes. In *Geodynamics of a Cordilleran Orogenic System: The Central Andes of Argentina and Northern Chile*. Geological Society of America. doi: [https://doi.org/10.1130/2015.1212\(03\)](https://doi.org/10.1130/2015.1212(03))
- Bello-González, J. P., Contreras-Reyes, E., & Arriagada, C. (2018). Predicted path for hotspot tracks off South America since Paleocene times: Tectonic implications of ridge-trench collision along the Andean margin. *Gondwana Research*, 64, 216–234. doi: <https://doi.org/10.1016/j.gr.2018.07.008>
- Boutelier, D. A., & Cruden, A. R. (2008). Impact of regional mantle flow on subducting plate geometry and interplate stress: insights from physical modelling. *Geophysical Journal International*, 174(2), 719–732. doi: <https://doi.org/10.1111/j.1365-246X.2008.03826.x>

- 338 Burd, A. I., Booker, J. R., Mackie, R., Favetto, A., & Pomposiello, M. C. (2014). Three-
 339 dimensional electrical conductivity in the mantle beneath the Payún Matrú Volcanic
 340 Field in the Andean backarc of Argentina near 36.5 S: Evidence for decapitation of a
 341 mantle plume by resurgent upper mantle shear during slab steepening. *Geophysical*
 342 *Journal International*, 198(2), 812–827. doi: <https://doi.org/10.1093/gji/ggu145>
- 343 Burd, A. I., Booker, J. R., Mackie, R., Pomposiello, M. C., & Favetto, A. (2013). Electrical
 344 conductivity of the pampean shallow subduction region of argentina near 33 s: Evi-
 345 dence for a slab window. *Geochemistry, Geophysics, Geosystems*, 14(8), 3192–3209.
 346 doi: <https://doi.org/10.1002/ggge.20213>
- 347 Celli, N. L., Lebedev, S., Schaeffer, A. J., Ravenna, M., & Gaina, C. (2020). The upper
 348 mantle beneath the South Atlantic Ocean, South America and Africa from waveform
 349 tomography with massive data sets. *Geophysical Journal International*, 221(1), 178-
 350 204. doi: <https://doi.org/10.1093/gji/ggz574>
- 351 Chen, Y. W., Wu, J., & Suppe, J. (2019). Southward propagation of Nazca subduction
 352 along the Andes. *Nature*, 565(7740), 441–447. doi: [https://doi.org/10.1038/s41586-](https://doi.org/10.1038/s41586-018-0860-1)
 353 [-018-0860-1](https://doi.org/10.1038/s41586-018-0860-1)
- 354 Cristallini, E. O., & Ramos, V. A. (2000). Thick-skinned and thin-skinned thrusting in the
 355 La Ramada fold and thrust belt: crustal evolution of the High Andes of San Juan,
 356 Argentina (32 SL). *Tectonophysics*, 317(3-4), 205–235. doi: [https://doi.org/10.1016/](https://doi.org/10.1016/S0040-1951(99)00276-0)
 357 [S0040-1951\(99\)00276-0](https://doi.org/10.1016/S0040-1951(99)00276-0)
- 358 Dai, L., Wang, L., Lou, D., Li, Z.-H., Dong, H., Ma, F., ... Yu, S. (2020). Slab rollback
 359 versus delamination: Contrasting fates of flat-slab subduction and implications for
 360 South China evolution in the Mesozoic. *Journal of Geophysical Research: Solid Earth*,
 361 125(4), e2019JB019164. doi: <https://doi.org/10.1029/2019JB019164>
- 362 D’Annunzio, M. C., Rubinstein, N., & Rabbia, O. (2018). Petrogenesis of the Gualcamayo
 363 Igneous Complex: Regional implications of Miocene magmatism in the Precordillera
 364 over the Pampean flat-slab segment, Argentina. *Journal of South American Earth*
 365 *Sciences*, 88, 16-28. doi: <https://doi.org/10.1016/j.jsames.2018.06.012>
- 366 Ekström, G., Nettles, M., & Dziewoński, A. (2012). The global CMT project 2004–2010:
 367 Centroid-moment tensors for 13,017 earthquakes. *Physics of the Earth and Planetary*
 368 *Interiors*, 200-201, 1 - 9. doi: <https://doi.org/10.1016/j.pepi.2012.04.002>
- 369 Engdahl, E. R., Di Giacomo, D., Sakarya, B., Gkarlaoui, C. G., Harris, J., & Storchak,
 370 D. A. (2020). ISC-EHB 1964–2016, an Improved Data Set for Studies of Earth
 371 Structure and Global Seismicity. *Earth and Space Science*, 7(1), e2019EA000897.
 372 doi: <https://doi.org/10.1029/2019EA000897>

- 373 Feng, M., Van der Lee, S., & Assumpção, M. (2007). Upper mantle structure of South
374 America from joint inversion of waveforms and fundamental mode group velocities
375 of Rayleigh waves. *Journal of Geophysical Research: Solid Earth*, 112(B4). doi:
376 <https://doi.org/10.1029/2006JB004449>
- 377 Fichtner, A., Kennett, B. L., Igel, H., & Bunge, H.-P. (2010). Full waveform tomography
378 for radially anisotropic structure: new insights into present and past states of the
379 Australasian upper mantle. *Earth and Planetary Science Letters*, 290(3-4), 270–280.
380 doi: <https://doi.org/10.1016/j.epsl.2009.12.003>
- 381 Fichtner, A., & Trampert, J. (2011). Resolution analysis in full waveform inversion. *Geo-*
382 *physical Journal International*, 187(3), 1604–1624. doi: [https://doi.org/10.1111/](https://doi.org/10.1111/j.1365-246X.2011.05218.x)
383 [j.1365-246X.2011.05218.x](https://doi.org/10.1111/j.1365-246X.2011.05218.x)
- 384 Gans, C. R., Beck, S. L., Zandt, G., Gilbert, H., Alvarado, P., Anderson, M., & Linkimer,
385 L. (2011). Continental and oceanic crustal structure of the Pampean flat slab re-
386 gion, western Argentina, using receiver function analysis: New high-resolution re-
387 sults. *Geophysical Journal International*, 186(1), 45–58. doi: [https://doi.org/10.1111/](https://doi.org/10.1111/j.1365-246X.2011.05023.x)
388 [j.1365-246X.2011.05023.x](https://doi.org/10.1111/j.1365-246X.2011.05023.x)
- 389 Gao, Y., Tilmann, F., van Herwaarden, D.-P., Thrastarson, S., Fichtner, A., Heit, B., ...
390 Schurr, B. (2021). Full Waveform Inversion beneath the Central Andes: Insight
391 into the dehydration of the Nazca slab and delamination of the back-arc lithosphere.
392 *Journal of Geophysical Research: Solid Earth*, 126(7), e2021JB021984. doi: [https://](https://doi.org/10.1029/2021JB021984)
393 doi.org/10.1029/2021JB021984
- 394 Gianni, G., Pesce, A., & Soler, S. (2018). Transient plate contraction between two simul-
395 taneous slab windows: Insights from Paleogene tectonics of the Patagonian Andes.
396 *Journal of Geodynamics*, 121, 64-75. doi: <https://doi.org/10.1016/j.jog.2018.07.008>
- 397 Goss, A. R., Kay, S., Mpodozis, C., & Singer, B. (2009). The Incapillo Caldera and
398 Dome Complex (~ 28 S, central Andes): A stranded magma chamber over a dying
399 arc. *Journal of volcanology and geothermal research*, 184(3-4), 389–404. doi: [https://](https://doi.org/10.1016/j.jvolgeores.2009.05.005)
400 doi.org/10.1016/j.jvolgeores.2009.05.005
- 401 Goss, A. R., Kay, S. M., & Mpodozis, C. (2011). The geochemistry of a dying continental
402 arc: the Incapillo Caldera and Dome Complex of the southernmost Central Andean
403 Volcanic Zone (~ 28 S). *Contributions to Mineralogy and Petrology*, 161(1), 101–128.
404 doi: <https://doi.org/10.1007/s00410-010-0523-1>
- 405 Gutscher, M.-A. (2018). Scraped by flat-slab subduction. *Nature Geoscience*, 11(12),
406 890–891. doi: <https://doi.org/10.1038/s41561-018-0270-x>
- 407 Gutscher, M.-A., Maury, R., Eissen, J.-P., & Bourdon, E. (2000). Can slab melting be

- caused by flat subduction? *Geology*, 28(6), 535–538.
- Haddon, A., & Porter, R. (2018). S-Wave Receiver Function Analysis of the Pampean Flat-Slab Region: Evidence for a Torn Slab. *Geochemistry, Geophysics, Geosystems*, 19(10), 4021–4034. doi: <https://doi.org/10.1029/2018GC007868>
- Haschke, M., Scheuber, E., Günther, A., & Reutter, K.-J. (2002). Evolutionary cycles during the Andean orogeny: repeated slab breakoff and flat subduction? *Terra nova*, 14(1), 49–55. doi: <https://doi.org/10.1046/j.1365-3121.2002.00387.x>
- Hayes, G. P., Moore, G. L., Portner, D. E., Hearne, M., Flamme, H., Furtney, M., & Smoczyk, G. M. (2018). Slab2, a comprehensive subduction zone geometry model. *Science*, 362(6410), 58–61. doi: <https://doi.org/10.1126/science.aat4723>
- Heit, B., Yuan, X., Bianchi, M., Sodoudi, F., & Kind, R. (2008). Crustal thickness estimation beneath the southern central Andes at 30°S and 36°S from S wave receiver function analysis. *Geophysical Journal International*, 174(1), 249–254. doi: <https://doi.org/10.1111/j.1365-246X.2008.03780.x>
- Hildreth, W., & Moorbath, S. (1988). Crustal contributions to arc magmatism in the Andes of central Chile. *Contributions to mineralogy and petrology*, 98(4), 455–489. doi: <https://doi.org/10.1007/BF00372365>
- Horton, B. K. (2018). Tectonic Regimes of the Central and Southern Andes: Responses to Variations in Plate Coupling During Subduction. *Tectonics*, 37(2), 402–429. doi: <https://doi.org/10.1002/2017TC004624>
- Hu, J., Faccenda, M., & Liu, L. (2017). Subduction-controlled mantle flow and seismic anisotropy in South America. *Earth and Planetary Science Letters*, 470, 13–24. doi: <https://doi.org/10.1016/j.epsl.2017.04.027>
- Hu, J., & Liu, L. (2016). Abnormal seismological and magmatic processes controlled by the tearing South American flat slabs. *Earth and Planetary Science Letters*, 450, 40–51. doi: <https://doi.org/10.1016/j.epsl.2016.06.019>
- Hu, J., Liu, L., Hermosillo, A., & Zhou, Q. (2016). Simulation of late Cenozoic South American flat-slab subduction using geodynamic models with data assimilation. *Earth and Planetary Science Letters*, 1–13. doi: <https://doi.org/10.1016/j.epsl.2016.01.011>
- Huangfu, P., Wang, Y., Cawood, P. A., Li, Z.-H., Fan, W., & Gerya, T. V. (2016). Thermo-mechanical controls of flat subduction: Insights from numerical modeling. *Gondwana Research*, 40, 170–183. doi: <https://doi.org/10.1016/j.gr.2016.08.012>
- Kay, R. W., & Kay, S. M. (2002). Andean adakites: three ways to make them. *Acta Petrologica Sinica*, 18(3), 303–311.
- Kay, S. M., & Abbruzzi, J. (1996). Magmatic evidence for Neogene lithospheric evolution

- 443 of the central Andean “flat-slab” between 30 S and 32 S. *Tectonophysics*, 259(1-3),
 444 15–28. doi: [https://doi.org/10.1016/0040-1951\(96\)00032-7](https://doi.org/10.1016/0040-1951(96)00032-7)
- 445 Kay, S. M., & Coira, B. L. (2009). Shallowing and steepening subduction zones, continental
 446 lithospheric loss, magmatism, and crustal flow under the Central Andean Altiplano-
 447 Puna Plateau. *Backbone of the Americas: shallow subduction, plateau uplift, and ridge
 448 and terrane collision, 204*, 229. doi: [https://doi.org/10.1130/2009.1204\(11\)](https://doi.org/10.1130/2009.1204(11))
- 449 Kay, S. M., & Mpodozis, C. (2002). Magmatism as a probe to the Neogene shallowing of
 450 the Nazca plate beneath the modern Chilean flat-slab. *Journal of South American
 451 Earth Sciences*, 15(1), 39–57. doi: [https://doi.org/10.1016/S0895-9811\(02\)00005-6](https://doi.org/10.1016/S0895-9811(02)00005-6)
- 452 Kendrick, E., Bevis, M., Smalley Jr, R., Brooks, B., Vargas, R. B., Lauria, E., & Fortes,
 453 L. P. S. (2003). The Nazca–South America Euler vector and its rate of change.
 454 *Journal of South American Earth Sciences*, 16(2), 125–131. doi: [https://doi.org/10.1016/S0895-9811\(03\)00028-2](https://doi.org/10.1016/S0895-9811(03)00028-2)
- 455
 456 Kopp, H., Flueh, E. R., Papenberg, C., & Klaeschen, D. (2004). Seismic investigations of the
 457 O’Higgins Seamount Group and Juan Fernández Ridge: Aseismic ridge emplacement
 458 and lithosphere hydration. *Tectonics*, 23(2), 1–21. doi: <https://doi.org/10.1029/2003TC001590>
- 459
 460 Krischer, L., Megies, T., Barsch, R., Beyreuther, M., Lecocq, T., Caudron, C., & Wasser-
 461 mann, J. (2015). ObsPy: a bridge for seismology into the scientific python ecosys-
 462 tem. *Computational Science & Discovery*, 8(1), 014003. doi: <https://doi.org/10.1088/1749-4699/8/1/014003>
- 463
 464 Li, C., Van Der Hilst, R. D., Engdahl, E. R., & Burdick, S. (2008). A new global model for
 465 P wave speed variations in Earth’s mantle. *Geochemistry, Geophysics, Geosystems*,
 466 9(5). doi: <https://doi.org/10.1029/2007GC001806>
- 467 Li, Z. (2020). Flat subduction versus big mantle wedge: contrasting modes for deep hy-
 468 dration and overriding craton modification. *Journal of Geophysical Research: Solid
 469 Earth*, 125(8). doi: <https://doi.org/10.1029/2020JB020018>
- 470 Li, Z., Xu, Z., & Gerya, T. (2011). Flat versus steep subduction: Contrasting modes for the
 471 formation and exhumation of high-to ultrahigh-pressure rocks in continental collision
 472 zones. *Earth and Planetary Science Letters*, 301(1-2), 65–77. doi: <https://doi.org/10.1016/j.epsl.2010.10.014>
- 473
 474 Lin, S. (2014). Three-dimensional mantle circulations and lateral slab deformation in the
 475 southern Chilean subduction zone. *Journal of Geophysical Research: Solid Earth*,
 476 119(4), 3879–3896. doi: <https://doi.org/10.1002/2013JB010864>
- 477 Linkimer, L., Beck, S., Zandt, G., Alvarado, P., Anderson, M., Gilbert, H., & Zhang, H.

- (2020). Lithospheric structure of the Pampean flat slab region from double-difference tomography. *Journal of South American Earth Sciences*, *97*, 102417. doi: <https://doi.org/10.1016/j.jsames.2019.102417>
- Liu, L., & Zhou, Q. (2015). Deep recycling of oceanic asthenosphere material during subduction. *Geophysical Research Letters*, *42*(7), 2204–2211. doi: <https://doi.org/10.1002/2015GL063633>
- Liu, S., & Currie, C. A. (2016). Farallon plate dynamics prior to the Laramide orogeny: Numerical models of flat subduction. *Tectonophysics*, *666*, 33–47. doi: <https://doi.org/10.1016/j.tecto.2015.10.010>
- Liu, X., & Currie, C. A. (2019). Influence of upper plate structure on flat-slab depth: Numerical modeling of subduction dynamics. *Journal of Geophysical Research: Solid Earth*, *124*(12), 13150–13167. doi: <https://doi.org/10.1029/2019JB018653>
- Lynner, C., Anderson, M. L., Portner, D. E., Beck, S. L., & Gilbert, H. (2017). Mantle flow through a tear in the Nazca slab inferred from shear wave splitting. *Geophysical Research Letters*, *44*(13), 6735–6742. doi: <https://doi.org/10.1002/2017GL074312>
- Manea, V. C., Manea, M., Ferrari, L., Orozco-Esquivel, T., Valenzuela, R., Husker, A., & Kostoglodov, V. (2017). A review of the geodynamic evolution of flat slab subduction in Mexico, Peru, and Chile. *Tectonophysics*, *695*, 27–52. doi: <https://doi.org/10.1016/j.tecto.2016.11.037>
- Manea, V. C., Pérez-Gussinyé, M., & Manea, M. (2012). Chilean flat slab subduction controlled by overriding plate thickness and trench rollback. *Geology*, *40*(1), 35–38. doi: <https://doi.org/10.1130/G32543.1>
- Marot, M., Monfret, T., Gerbault, M., Nolet, G., Ranalli, G., & Pardo, M. (2014). Flat versus normal subduction zones: A comparison based on 3-D regional traveltimes tomography and petrological modelling of central Chile and western Argentina (29°–35°S). *Geophysical Journal International*, *199*(3), 1633–1654. doi: <https://doi.org/10.1093/gji/ggu355>
- Mohammadzakeri, A., Sigloch, K., Hosseini, K., & Mihalynuk, M. G. (2021). Subducted Lithosphere Under South America From Multifrequency P Wave Tomography. *Journal of Geophysical Research: Solid Earth*, *126*(6), e2020JB020704. doi: <https://doi.org/10.1029/2020JB020704>
- Obayashi, M., Yoshimitsu, J., Nolet, G., Fukao, Y., Shiobara, H., Sugioka, H., . . . Gao, Y. (2013). Finite frequency whole mantle P wave tomography: Improvement of subducted slab images. *Geophysical Research Letters*, *40*(21), 5652–5657.
- Pesicek, J., Engdahl, E., Thurber, C., DeShon, H., & Lange, D. (2012). Mantle subducting

- slab structure in the region of the 2010 M 8.8 Maule earthquake (30–40 S), Chile. *Geophysical Journal International*, 191(1), 317–324. doi: <https://doi.org/10.1111/j.1365-246X.2012.05624.x>
- Piceda, C. R., Wenderoth, M. S., Dacal, M. L. G., Bott, J., Prezzi, C. B., & Strecker, M. R. (2020). Lithospheric density structure of the Southern Central Andes constrained by 3D data-integrative gravity modelling. *International Journal of Earth Sciences*, 1–27. doi: <https://doi.org/10.1007/s00531-020-01962-1>
- Porter, R., Gilbert, H., Zandt, G., Beck, S., Warren, L., Calkins, J., . . . Anderson, M. (2012). Shear wave velocities in the Pampean flat-slab region from Rayleigh wave tomography: Implications for slab and upper mantle hydration. *Journal of Geophysical Research B: Solid Earth*, 117(11), 1–21. doi: <https://doi.org/10.1029/2012JB009350>
- Portner, D. E., Beck, S., Zandt, G., & Scire, A. (2017). The nature of subslab slow velocity anomalies beneath South America. *Geophysical Research Letters*, 44(10), 4747–4755. doi: <https://doi.org/10.1002/2017GL073106>
- Portner, D. E., Rodríguez, E. E., Beck, S. L., Zandt, G., Scire, A., Rocha, M. P., . . . Alvarado, P. (2020). Detailed Structure of the Subducted Nazca Slab into the Lower Mantle Derived From Continent-Scale Teleseismic P Wave Tomography. *Journal of Geophysical Research: Solid Earth*, 125(5). doi: <https://doi.org/10.1029/2019JB017884>
- Ramos, V. A., Cristallini, E. O., & Pérez, D. J. (2002). The Pampean flat-slab of the Central Andes. *Journal of South American earth sciences*, 15(1), 59–78. doi: [https://doi.org/10.1016/S0895-9811\(02\)00006-8](https://doi.org/10.1016/S0895-9811(02)00006-8)
- Ramos, V. A., & Folguera, A. (2009). Andean flat-slab subduction through time. *Geological Society, London, Special Publications*, 327(1), 31–54. doi: <https://doi.org/10.1144/SP327.3>
- Ramos, V. A., & Folguera, A. (2011). Payenia volcanic province in the Southern Andes: An appraisal of an exceptional Quaternary tectonic setting. *Journal of Volcanology and geothermal Research*, 201(1-4), 53–64. doi: <https://doi.org/10.1016/j.jvolgeores.2010.09.008>
- Ranero, C. R., Villaseñor, A., Phipps Morgan, J., & Weinrebe, W. (2005). Relationship between bend-faulting at trenches and intermediate-depth seismicity. *Geochemistry, Geophysics, Geosystems*, 6(12). doi: <http://dx.doi.org/10.1029/2005GC000997>
- Ritsema, J., van Heijst, H. J., & Woodhouse, J. H. (2004). Global transition zone tomography. *Journal of Geophysical Research: Solid Earth*, 109(B2). doi: <https://doi.org/10.1029/2003JB002610>

- 548 Rivadeneyra-Vera, C., Bianchi, M., Assumpção, M., Cedraz, V., Julià, J., Rodríguez, M.,
549 ... others (2019). An updated crustal thickness map of central South America based
550 on receiver function measurements in the region of the Chaco, Pantanal, and Paraná
551 Basins, southwestern Brazil. *Journal of Geophysical Research: Solid Earth*, 124(8),
552 8491–8505. doi: <https://doi.org/10.1029/2018JB016811>
- 553 Rodríguez, E. E., Portner, D. E., Beck, S. L., Rocha, M. P., Bianchi, M. B., Assumpção,
554 M., ... Lynner, C. (2021). Mantle dynamics of the Andean Subduction Zone from
555 continent-scale teleseismic S-wave tomography. *Geophysical Journal International*,
556 224(3), 1553–1571. doi: <https://doi.org/10.1093/gji/ggaa536>
- 557 Rodríguez-González, J., Negredo, A. M., & Billen, M. I. (2012). The role of the overrid-
558 ing plate thermal state on slab dip variability and on the occurrence of flat subduc-
559 tion. *Geochemistry, Geophysics, Geosystems*, 13(1). doi: [https://doi.org/10.1029/](https://doi.org/10.1029/2011GC003859)
560 2011GC003859
- 561 Rodríguez-González, J., Negredo, A. M., & Carminati, E. (2014). Slab–mantle flow inter-
562 action: influence on subduction dynamics and duration. *Terra Nova*, 26(4), 265–272.
563 doi: <https://doi.org/10.1111/ter.12095>
- 564 Sánchez, M. A., García, H. P., Acosta, G., Gianni, G. M., Gonzalez, M. A., Ariza, J. P.,
565 ... Folguera, A. (2019). Thermal and lithospheric structure of the Chilean-Pampean
566 flat-slab from gravity and magnetic data. In *Andean tectonics* (pp. 487–507). Elsevier.
567 doi: <https://doi.org/10.1016/B978-0-12-816009-1.00005-8>
- 568 Schepers, G., Van Hinsbergen, D. J., Spakman, W., Kesters, M. E., Boschman, L. M.,
569 & McQuarrie, N. (2017). South-American plate advance and forced Andean trench
570 retreat as drivers for transient flat subduction episodes. *Nature Communications*,
571 8(0316), 1–9. doi: <https://doi.org/10.1038/ncomms15249>
- 572 Sippl, C., Moreno, M., & Benavente, R. (2020). Microseismicity appears to outline highly
573 coupled regions on the Central Chile megathrust. *EarthArXiv*. doi: [https://doi.org/](https://doi.org/10.31223/X56S3B)
574 10.31223/X56S3B
- 575 Tao, K., Grand, S. P., & Niu, F. (2018). Seismic Structure of the Upper Mantle Beneath
576 Eastern Asia From Full Waveform Seismic Tomography. *Geochemistry, Geophysics,*
577 *Geosystems*, 19(8), 2732–2763. doi: <https://doi.org/10.1029/2018GC007460>
- 578 Tape, C., Liu, Q., Maggi, A., & Tromp, J. (2010). Seismic tomography of the southern
579 California crust based on spectral-element and adjoint methods. *Geophysical Journal*
580 *International*, 180(1), 433–462. doi: <https://doi.org/10.1111/j.1365-246X.2009.04429>
581 .x
- 582 Tassara, A., Götze, H.-J., Schmidt, S., & Hackney, R. (2006). Three-dimensional density

- 583 model of the Nazca plate and the Andean continental margin. *Journal of Geophysical*
 584 *Research: Solid Earth*, 111(B9). doi: <https://doi.org/10.1029/2005JB003976>
- 585 Wagner, L. S., Beck, S., & Zandt, G. (2005). Upper mantle structure in the south central
 586 Chilean subduction zone (30 to 36 s). *Journal of Geophysical Research: Solid Earth*,
 587 110(B1). doi: <https://doi.org/10.1029/2004JB003238>
- 588 Wagner, L. S., Caddick, M. J., Kumar, A., Beck, S. L., & Long, M. D. (2020). Effects
 589 of Oceanic Crustal Thickness on Intermediate Depth Seismicity. *Frontiers in Earth*
 590 *Science*, 8(July). doi: <https://doi.org/10.3389/feart.2020.00244>
- 591 Ward, K. M., Delph, J. R., Zandt, G., Beck, S. L., & Ducea, M. N. (2017). Magmatic
 592 evolution of a Cordilleran flare-up and its role in the creation of silicic crust. *Scientific*
 593 *Reports*, 7(1), 1–8. doi: <https://doi.org/10.1038/s41598-017-09015-5>
- 594 Ward, K. M., Porter, R. C., Zandt, G., Beck, S. L., Wagner, L. S., Minaya, E., & Tavera,
 595 H. (2013). Ambient noise tomography across the Central Andes. *Geophysical Journal*
 596 *International*, 194(3), 1559–1573. doi: <https://doi.org/10.1093/gji/ggt166>
- 597 Ward, K. M., Zandt, G., Beck, S. L., Christensen, D. H., & McFarlin, H. (2014). Seismic
 598 imaging of the magmatic underpinnings beneath the altiplano-puna volcanic complex
 599 from the joint inversion of surface wave dispersion and receiver functions. *Earth and*
 600 *Planetary Science Letters*, 404, 43 – 53. doi: <https://doi.org/10.1016/j.epsl.2014.07>
 601 .022
- 602 Yáñez, G. A., Ranero, C. R., Von Huene, R., & Díaz, J. (2001). Magnetic anomaly interpre-
 603 tation across the southern central Andes (32°–34°S): The role of the Juan Fernández
 604 Ridge in the late Tertiary evolution of the margin. *Journal of Geophysical Research:*
 605 *Solid Earth*, 106(B4), 6325–6345. doi: <https://doi.org/10.1029/2000jb900337>
- 606 Yuan, X., Sobolev, S. V., Kind, R., Oncken, O., Bock, G., Asch, G., . . . Comte, D. (2000).
 607 Subduction and collision processes in the Central Andes constrained by converted
 608 seismic phases. *Nature*, 408(6815), 958–961. doi: 10.1038/35050073

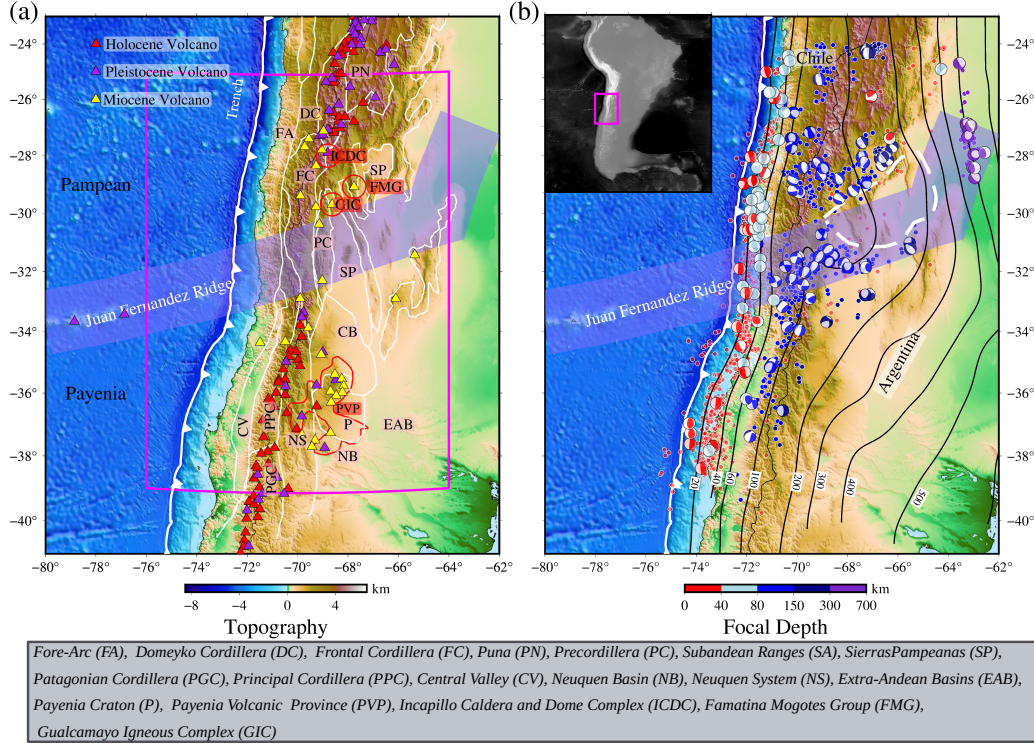


Figure 1. (a) Map of major morphotectonic provinces (modified from Tassara et al. (2006); Picada et al. (2020)). Red solid line denotes the Payenia Volcanic Province (Ramos & Folguera, 2011). White saw-tooth line denotes the trench. (b) Map showing focal mechanisms of the earthquakes used for FWI. Color-coded circles represent the seismicity (magnitude $> M_w 4.0$) retrieved from the ISC-EHB catalog (Engdahl et al., 2020). Black solid lines denote the Nazca slab contours from Slab 2.0 (Hayes et al., 2018). Inset map marks the position of our study region. Topography data is retrieved from ETOPO1 Global Relief Model (Amante & Eakins, 2009).

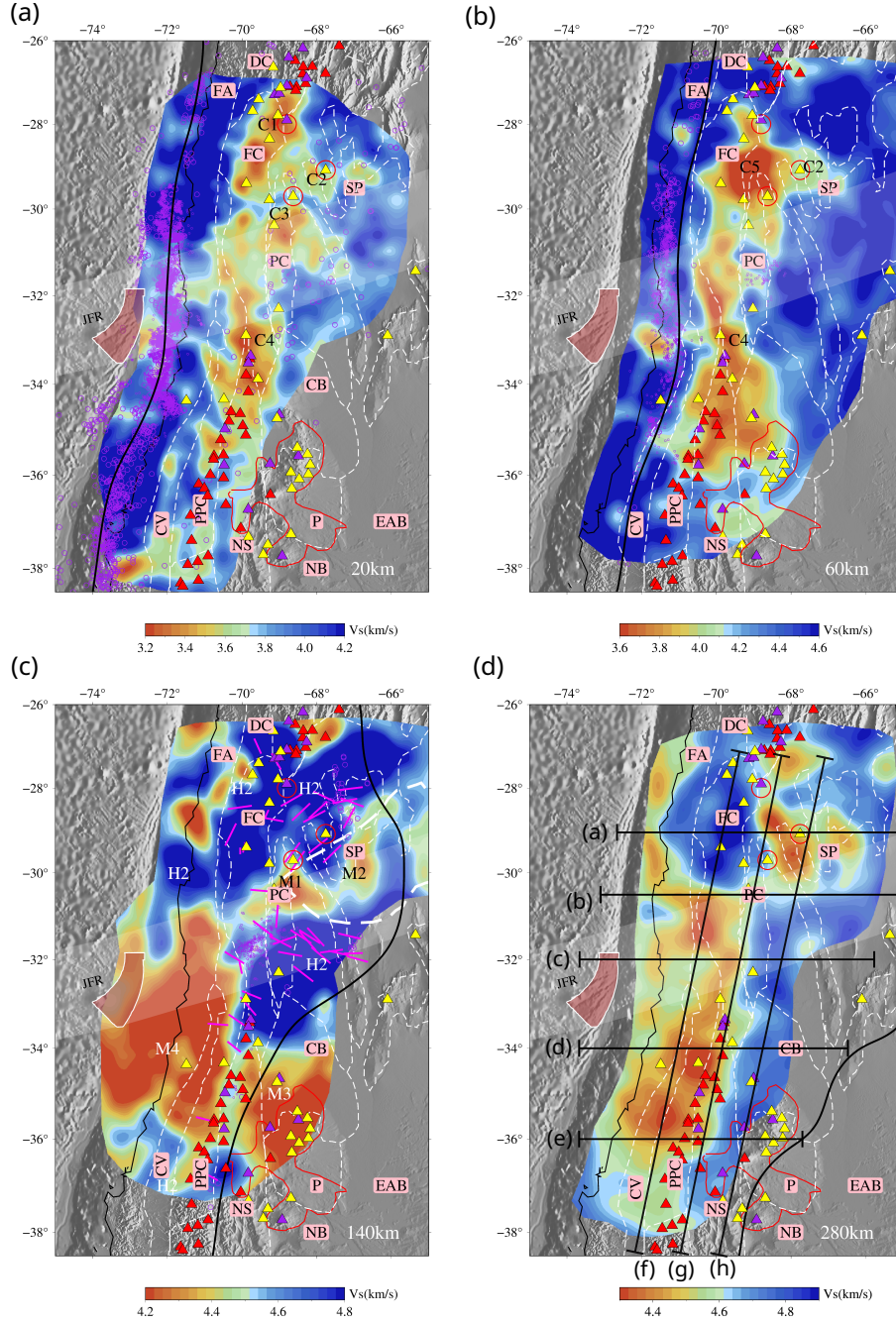


Figure 2. Horizontal slices for isotropic V_S at 20 km (a), 60 km (b), 140 km (c), and 280 km (d). In (c) T (tension) axes from GCMT focal mechanism solutions (Ekström et al., 2012) for earthquakes between 120 and 150 km depth with magnitude $M_W > 5.0$ are indicated by magenta bars. The large and small magenta circles are seismicity from ISC-EHB catalog and the relocated catalog from Sippl et al. (2020), respectively, and within 10 km of the nominal depth of the slice. The pink shaded area off-shore indicates the position of the weakened oceanic lithosphere detected by Kopp et al. (2004) along the JFR. Solid black lines denote the top of the slab according to Slab 2.0 (Hayes et al., 2018) at the depth of the slice. Black straight lines in (d) denote the positions of

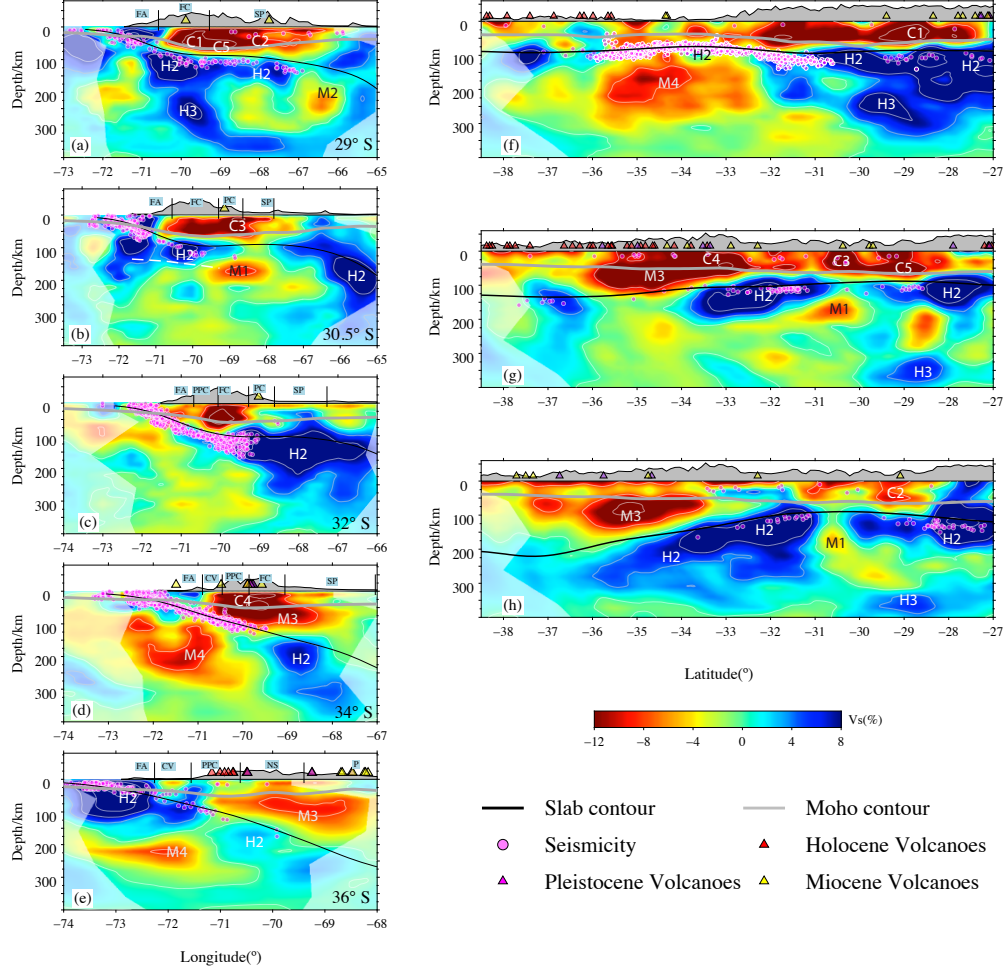


Figure 3. Cross-sections of isotropic V_S perturbation relative to the reference 1D V_S defined in Figure S3. (see Figure 2d for profile locations). Thick solid black lines denote the continental Moho (Rivadeneyra-Vera et al., 2019) and thin solid black lines denote the slab contour from Slab 2.0 (Hayes et al., 2018). The thick white dashed line in b denotes the oceanic LAB from receiver function (Heit et al., 2008). Magenta dots in b-d denote the seismicity relocated by Sippl et al. (2020) and in other profiles are retrieved from ISC-EHB catalog.

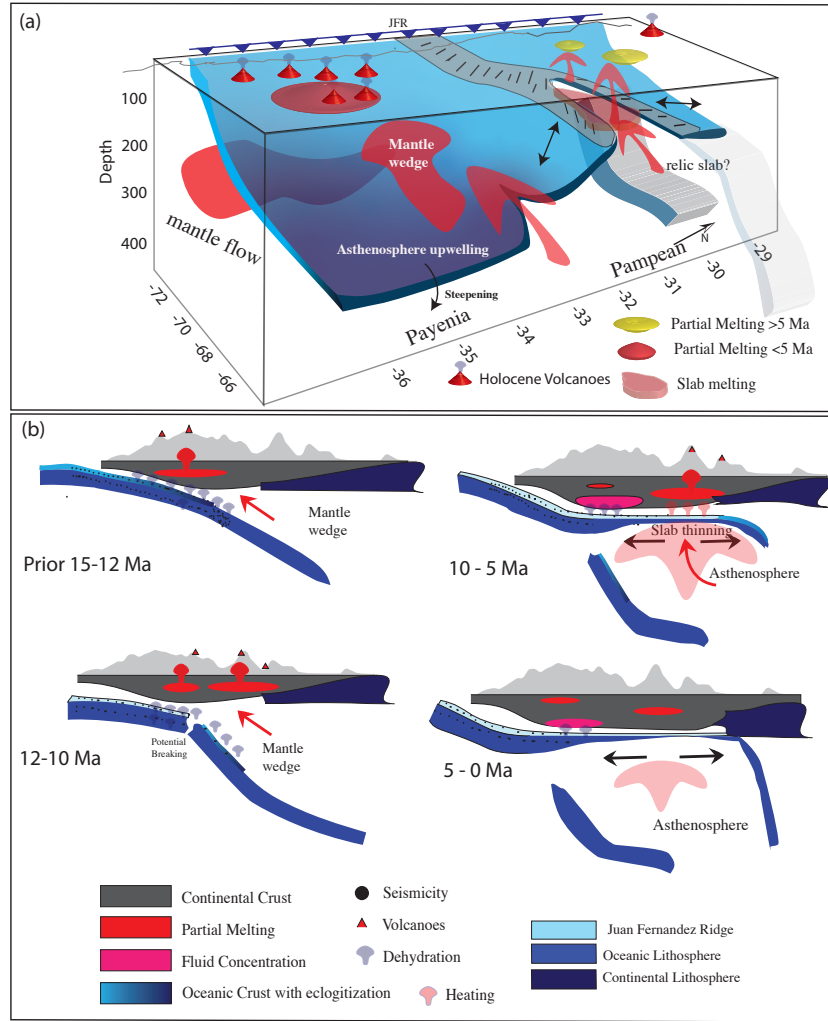


Figure 4. (a) Schematic representation of the current Nazca slab configuration west of 66°W. Gray zone with short bars indicates the inland projection of the Juan Fernandez Ridge. South of 33°S the Nazca plate subducts steeply in the Payenia segment. (b) Proposed sequence of the steep to flat slab subduction evolution along 29°S since 12 Ma, which can explain the observed pattern of sub-slab anomalies.